

Custom Soft Robotic Gripper Sensor Skins for Haptic Object Visualization

Benjamin Shih¹, Dylan Drotman¹, Caleb Christianson², Zhaoyuan Huo¹, Ruffin White³,
Henrik I. Christensen³, Michael T. Tolley¹

Abstract—Robots are becoming increasingly prevalent in our society in forms where they are assisting or interacting with humans in a variety of environments, and thus they must have the ability to sense and detect objects by touch. An ongoing challenge for soft robots has been incorporating flexible sensors that can recognize complex motions and close the loop for tactile sensing. We present sensor skins that enable haptic object visualization when integrated on a soft robotic gripper that can twist an object. First, we investigate how the design of the actuator modules impact bend angle and motion. Each soft finger is molded using a silicone elastomer, and consists of three pneumatic chambers which can be inflated independently to achieve a range of complex motions. Three fingers are combined to form a soft robotic gripper. Then, we manufacture and attach modular, flexible sensory skins on each finger to measure deformation and contact. These sensor measurements are used in conjunction with an analytical model to construct 2D and 3D tactile object models. Our results are a step towards soft robot grippers capable of a complex range of motions and proprioception, which will help future robots better understand the environments with which they interact, and has the potential to increase physical safety in human-robot interaction. Please see the accompanying video for additional details.

I. INTRODUCTION

In the absence of visual information, humans can readily identify unknown objects through touch alone. However, the same task is a major challenge for typical robotic systems, although it would be useful in many situations including industrial automation, and human-robot interaction. In particular, rigid grippers require special care and dexterity to manipulate delicate objects, especially unknown ones, without damage. By contrast, robotic grippers that are soft, composed of compliant materials like silicone elastomers, are suitable candidates for tactile interaction with fragile objects or even humans. Furthermore, adding sensing to these soft robotic grippers can enable new capabilities such as haptic identification and modeling.

The human ability to rotate an object in-hand is an important capability, and key for haptic object recognition. As more robots enter and co-exist in a world where objects are designed for humans, in-hand manipulation becomes an increasingly important ability for robots to mimic. However, to our knowledge, this capability has not yet been replicated in a soft robot gripper with integrated sensing.

¹ Department of Mechanical and Aerospace Engineering at University of California, San Diego.

² Department of NanoEngineering at University of California, San Diego.

³ Department of Computer Science and Engineering at University of California, San Diego.

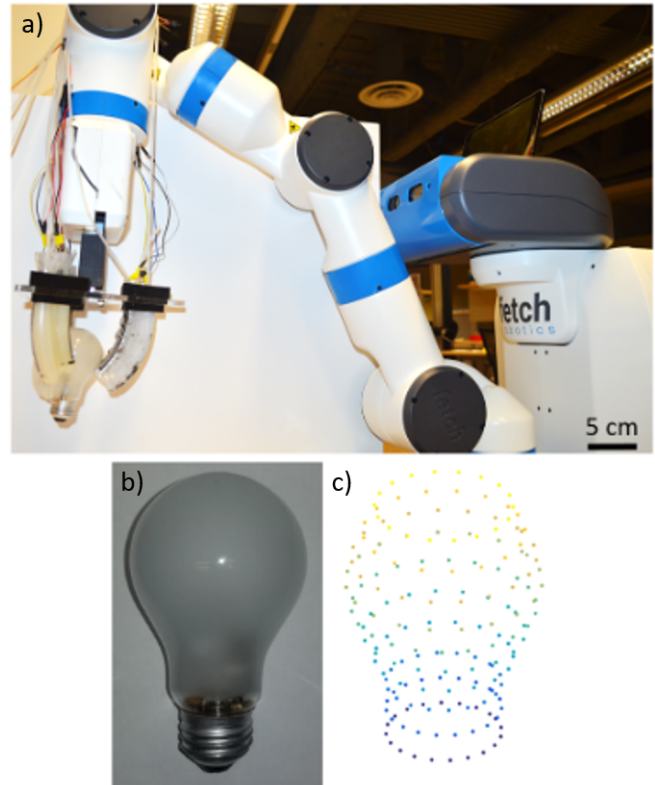


Fig. 1: Our proposed soft pneumatic gripper with internal sensing attached to a robot arm. a) Using the soft gripper and robot arm to pick up a light bulb. b) Light bulb that we used to generate the visualization. c) 3D haptic object visualization generated by our gripper, with our data plotted in a 2D view. We estimated where the gripper contacted the object via sensor reading and each color represents a different height.

We developed soft robotic fingers that can sense their deflections during actuation, sense fingertip contact, and build 3D outline models of unknown objects. We improve upon existing approaches by synthesizing hardware and software components and creating soft, twisting fingers with internal sensing to estimate unknown object outlines using touch. Finally, we put our soft gripper onto a commercial robot arm (Fetch, Fetch Robotics Inc.) to demonstrate its capability to build 3D tactile object models.

In this paper, we present:

- An approach for designing, fabricating, and using flex-

ible, modular skins with custom geometries and sensor layouts for proprioception and exteroception.

- Sensorized soft pneumatic fingers capable of twisting. When multiple fingers are combined into a gripper, we can rotate objects in-hand when they are fixed along a central axis.
- A method for using haptic information obtained from these soft pneumatic fingers to collect point clouds for objects.

II. RELATED WORK

By altering the fundamental assumption that a robot consists of a kinematic chain of rigid links, we sacrifice characteristics such as precisely predictable dynamics and strength in exchange for compliance and the ability to handle fragile objects from a materials standpoint. Recent review papers [1]–[4] have discussed how robot designers can replace traditionally rigid robot components with compliant materials. Doing so improves locomotion in rough terrain [5] and enables safe physical contact in human-robot interaction [6]. These new design principles have the potential to unlock a technological change in the way we design robots.

Unlike rigid grippers, soft manipulators are capable of conforming to objects of different shapes and sizes, typically with minimal changes in hardware and software. Zhao et al. developed a robot gripper with soft fingers using waveguide sensors that can pick up both hard and soft objects and feel their textures [7]. Homberg et al. clustered sensor readings in their gripper to identify correspondences to finger configurations, and used this information to classify unknown objects [8]. Deimel and Brock created a soft hand made primarily from silicone [9]. On a mm scale, Suzumori et al. developed flexible microactuators capable of a twisting action to loosen and tighten small screws [10].

Current soft grippers rely primarily on external sensing to estimate location in space. In contrast, biological fingers rely on a combination of internal and external sensing, such as using both vision and touch for localization and object recognition [11]. Many different types of sensors are available for detecting contact [12]. Multiple groups have created actuators that can sense, grasp, and touch using liquid metal strain sensors [13], [14]. Using a similar manufacturing process, Muth et al. embedded conductive material using 3D printers to deposit traces within highly stretchable elastomers [15]. Kim et al. 3D printed pockets of air that sensed contact through deviations in pressure [16].

Fingers with tactile-based internal sensing can be used to identify unknown objects through touch. Okamura et al. [17] analyzed how rigid robotic fingers with soft, force-sensing fingertips can be used to explore unknown objects via dexterous manipulation. An example of soft haptics is Sonar and Paik’s pneumatic haptic feedback device where they embedded sensitive piezo ceramic sensors into thin silicone layers [18]. In addition, research using rigid grippers has also studied methods for classifying objects from touch [19]–[21], while other work has studied how to combine tactile sensing

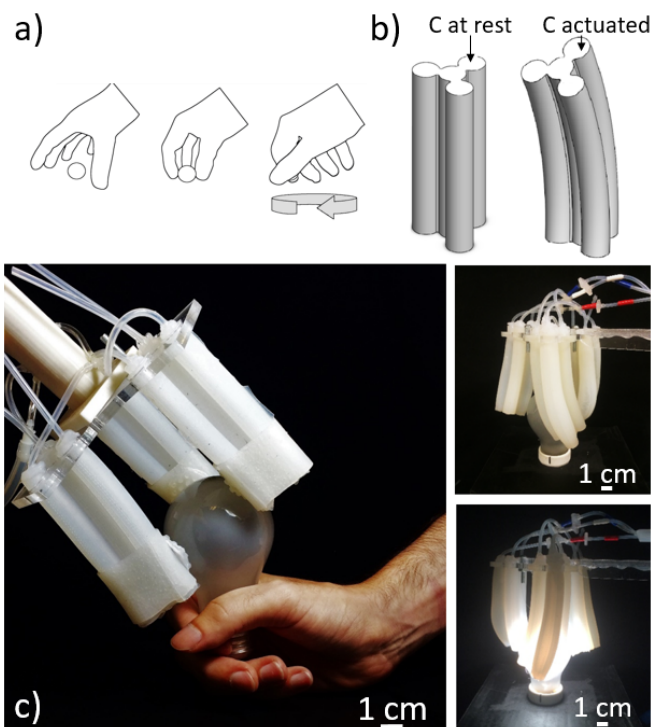


Fig. 2: Dexterous soft gripper capable of safely handling delicate objects under uncertainty. a) Side view of human hand grasping and twisting a round object, which inspired our design for in-hand manipulation. b) Visual model of actuator in resting state (left), and when chamber C is inflated (right). c) Soft gripper handling, manipulating, and rotating a light bulb.

with in-hand manipulation [22] and define types of in-hand manipulation [23].

III. DESIGN

A. Actuator Module Design

Soft pneumatic actuators operate by applying air pressure inside of a sealed chamber, resulting in motion. Typically, some asymmetry in the structure, material, or actuation of these chambers directs the motion. We present a simple actuator module composed of three sealed chambers oriented longitudinally, with independent control of the pressure in each chamber, modeled on a previous design by Suzumori et al. [10] and other three chamber designs [5], [24]. Each chamber expands radially and longitudinally when inflated and the outer edge of the chamber lengthens. The central portion of the actuator acts as a constraint on the chamber, and thus the longitudinal motion of the chamber results in bending (Fig. 2). We can achieve a wide range of positions by inflating combinations of the three chambers – the workspace resulting from inflation of multiple chambers is a set of nested hemispheres. Inflating multiple chambers simultaneously enables a twisting motion.

B. Sensor Design

We next augmented our actuator modules with sensing capabilities. Previously, sensors have been directly adhered to or embedded within the actuator modules [7], [13], [14]. However, users or designers may want to change the arrangement of sensors on the skin for customizability and adaptability [25]. In addition, the lifetime of the sensors often differs greatly from the lifetime of the actuators because the actuators tend to form hernias over time. Other groups have addressed this challenge by reinforcing with fibers [9] or fabricating with foam [26]. Our approach was to design a modular, reusable sensor skin that would be customizable and scalable to arbitrary surfaces.

For the sensor skins described in this paper, we placed one stretch sensor longitudinally along the outside of each of the pneumatic chambers of the actuator to measure bending and one strain sensor in the space between two chambers at the fingertip to detect contact.

C. Gripper Design

The gripper is composed of three soft actuator modules mounted to a laser cut acrylic frame. The three actuator modules are situated so that they are radially symmetric around a central axis represented by the palm of the gripper. By executing the proper sequence of pneumatic actuation, the gripper can manipulate a variety of objects (Fig. 3).

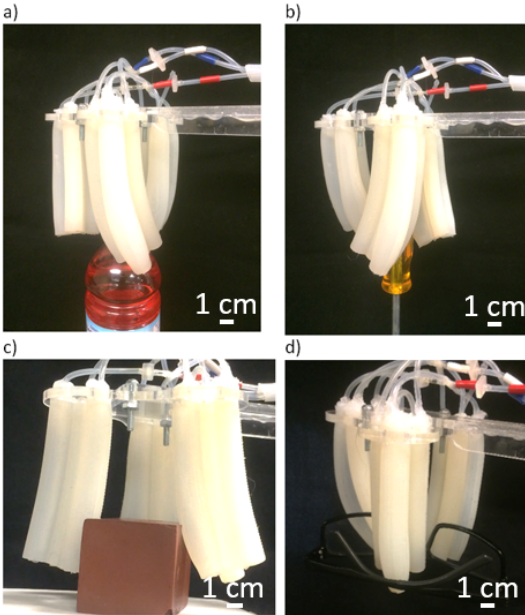


Fig. 3: Our proposed soft gripper design is capable of performing a range of complex manipulation tasks, including: a) unscrewing a bottle cap, b) rotating a screw driver, c) opening up its grasp area to manipulate a larger box, and d) grasping complex shapes such as a pair of glasses.

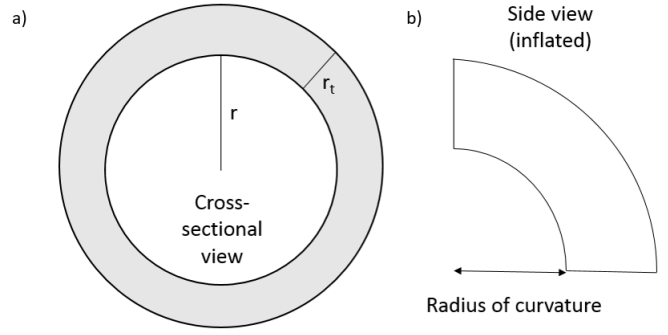


Fig. 4: Schematic of the 2D analytical model of our actuator. a) Cross-sectional view. b) Side view, where the actuator is inflated, bent, and at equilibrium.

IV. ANALYTICAL MODEL

A. 2D Actuator Model

Our 2D model uses a force balance between expansion and elastic compression forces at steady state, as described by Farrow et al. [13]. In this model, we assume that: 1) when a single chamber inflates, only the outer edge of the chamber extends; 2) the actuator deforms uniformly and thus maintains constant curvature; 3) the actuator is radially symmetric (Fig. 4); 4) pressure on the end caps is a negligible fringe effect; 5) radial expansion is negligible compared to longitudinal expansion; and 6) the actuator is hanging vertically.

Our model studies the actuator curvature in 2D only because we only need to know the in-plane bending of the actuator for haptic modeling. Previous work has explored modeling three-chambered actuators in 3D [10], but for chambers with different geometry and scale. Translating these models to 3D for our actuators lies outside the scope of this paper as it is not required for the current goals.

The expansion force can be computed as:

$$\begin{aligned} F_{expand} &= \int_0^{2\pi} \int_r^{r+r_t} Pr dr d\theta \\ &= P\pi(2rr_t + r_t^2) \end{aligned} \quad (1)$$

where r is the radius of the internal chamber, r_t is the thickness of the actuator walls, and P is the internal pressure of the chamber.

Using Hooke's Law for elastic materials, we computed the compression force as:

$$\begin{aligned} F_{contract} &= k\Delta x \rightarrow \frac{EA_0}{L_0}\Delta L \\ &= \int \frac{E}{L}\Delta L(r, \theta) dA \end{aligned} \quad (2)$$

where E is the Young's modulus of the material of the actuator, A_0 is the initial cross-sectional area, L_0 is the initial length of the actuator, and ΔL is the extension of the actuator which can be described here as a function of r and θ .

From the side-view geometry, $\Delta L(r, \theta)$ can be written as $2r\frac{L}{C}$. These forces are balanced at equilibrium and thus by substituting and setting $F_{expand} = F_{contract}$, we can solve for both the curvature κ and radius of curvature K of the actuator:

$$\begin{aligned}\kappa &= \frac{4E(3rr_t + 3r^2 + r_t^2)}{3P(2r + r_t)} \\ K &= \frac{1}{\kappa} \\ &= \frac{3P(2r + r_t)}{4E(3rr_t + 3r^2 + r_t^2)}\end{aligned}\quad (3)$$

Taking mass effect into account:

$$\begin{aligned}F_{mass} &= \int g\rho A\Delta h \cos\theta d\theta = mg \sin\theta \\ F_{mass} + F_{contract} &= F_{expand}\end{aligned}\quad (4)$$

From the above equation, the relationship for bend angle vs. pressure is:

$$P = \frac{2E}{L}(r + r_t)\theta + mg\sin\theta \quad (5)$$

B. Sensor Model

We modeled the strain of the sensor by analyzing the relationship between the resistance and the extended length of the sensor. In this model, we assume that: 1) the sensor experiences no deformations other than lengthwise extension from length l to $l + \Delta l$; 2) negligible fringe and edge effects of the sensor; and 3) the conductive material inside the sensor is incompressible and thus maintains a constant volume.

We start with the general formula for resistance, $R = \frac{\rho l}{A}$. Since the sensor has constant volume, we can calculate the cross sectional area after stretching as:

$$A_{stretched} = \frac{l}{l + \Delta l}A \quad (6)$$

Plugging the stretched length into the general resistance equation, we obtain:

$$R = \frac{2\rho}{A}\left(\frac{\Delta l^2}{l} + 2\Delta l + l\right) \quad (7)$$

The factor 2 in front of ρ is due to the parallel construction of two identical sensors. Thus, we obtained a second order polynomial relationship between resistance and the change in length.

V. FABRICATION

A. Fabrication of Actuator Module

We fabricated the actuators using a five step procedure: 1) filled the mold with silicone (Fig. 5a), 2) inserted the inner chamber rods (Fig. 5b), 3) left the actuator to cure (Fig. 5c), 4) removed the actuator from the mold (Fig. 5d), and 5) sealed the actuator openings with tubing and silicone epoxy (Fig. 5e).

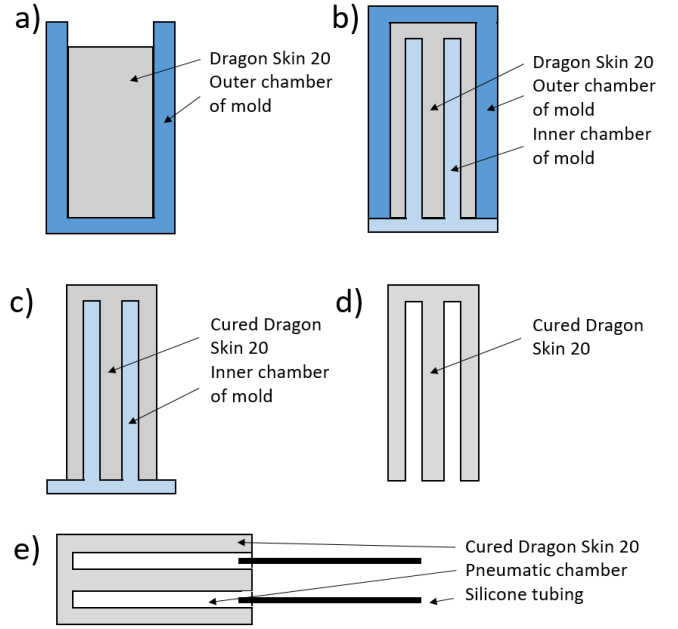


Fig. 5: Schematic of our soft actuator module fabrication process, based on retractable-pin casting [27] – side view, with only two chambers shown. Steps: a) Fill outer chamber of the mold with silicone. b) Insert inner chamber of the mold into the silicone and outer chamber of the mold. c) After the silicone cures, remove the outer chamber of the mold. d) Next, remove the inner chamber of the mold, leaving behind chambers in the silicone. e) Insert tubing and seal the pneumatic chambers.

Using a photopolymer resin (Veroclear, Stratasys Objet350 Connex3), we 3D printed actuator molds which consisted of five pieces that encapsulate and shape the silicone during the curing process. We found that the use of translucent molds made with a high precision 3D printer significantly improved fabrication yields as compared to the use of opaque molds printed on desktop fused deposition modeling printers, as it allowed us to easily resolve molding problems like leaks or bubbles. The silicone was a commercial, two-part elastomer compound (Dragon Skin 20, Smooth-On Inc.).

B. Fabrication of Sensor Skin

We made sensors with conductive-polydimethylsiloxane (cPDMS) traces (Fig. 6). First, we dispersed multiwall carbon nanotubes (MWCNT) (30-50 nm diameter, Cheap Tubes, Inc.) in toluene by mixing with a stir bar for two hours. We then added PDMS base (Sylgard 184, 3M) to achieve 12% MWCNT loading by weight, which is expected to result in a conductivity of approximately 6 S/m [28]. We continued to stir the cPDMS overnight at 90 °C to allow the remaining toluene to evaporate. We then spin-coated a thin (approximately 0.05 mm thick) layer of silicone elastomer (Dragon Skin 10, Smooth-On Inc) onto a rigid substrate to form the lower layer of the sensing skin. We used Dragon Skin 10 as it has a lower shore value than the actuator

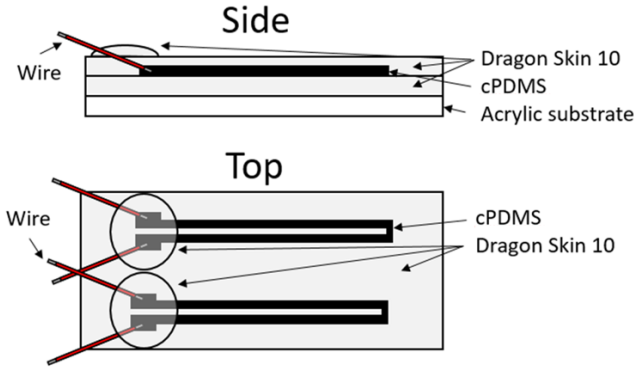


Fig. 6: Schematic of sensor fabrication process. A conductive silicone is embedded within thin layers of non-conductive silicone. We control the thickness of the layers via spin coating and the trace patterns are made via masking.

material, reducing the effect of the sensors on the overall stiffness of the actuator modules. We patterned a mask for the trace using silicone adhesive transfer tape via a digital laser machining system. Then, we removed one of the carrier layers of the tape, exposing one side of the adhesive, and affixed the adhesive to the layer of silicone elastomer. We next used a doctor blade to apply cPDMS to the mask, resulting in a trace thickness of approximately $100 \mu\text{m}$. We then removed the second carrier layer, applied wire leads to the conductive traces, and encapsulated the traces with a final layer of silicone elastomer.

C. Assembly of Finger Module

We formed our soft fingers by wrapping each actuator with a sensor skin (Fig. 7). We assume that there is no slipping between the skin and fingers due to the high coefficient of friction between the silicone elastomers. Each finger on the gripper has three degrees of freedom, which enable both bending and twisting. Three strain sensors in total are located on each of the outer inflating chambers. This positioning allows measurement of the actuator's bend in each direction. In addition, the fingertip strain sensor detects contact. The fingers are controlled using an open source fluidic control board [29]. We explore the advantages of a system that has both of these properties by conducting tactile object modeling experiments on various shapes to compare the visualization results (Section VI-B, VI-C).

VI. RESULTS

A. Experimental Validation

In order to explore the design space of actuator chamber sizes and the resulting pressures required for actuation, we tested two actuator designs with inner diameters of 5.08 mm (0.2 in) and 6.35 mm (0.25 in). We validated our model by comparing our bend angle measurements as a function of pressure (Fig. 8) and measured the bend angles by recording the angle of the end effector with respect to the horizon [5]. By observation from equation 5, the magnitude of mg is

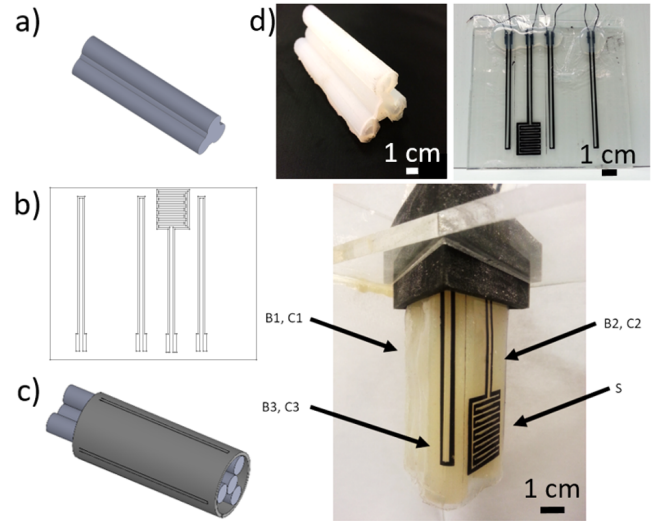


Fig. 7: Schematic and manufacturing process for the finger modules. a) Mold the actuator modules from silicone elastomer. b) Sensor skins are fabricated as flat sheets with trace patterns that match the geometry of the actuator. c) The skins are rolled up, sealed, and worn as modular sleeves on the actuator. d) Cured silicone actuator module after it has been removed from the mold. e) Flexible, silicone strain sensors which form a skin around the actuator module. f) Completed finger that integrates both actuator and sensor skin, where C_i are the pneumatic chambers, B_i are the flexible sensors that measure the actuator bend, and S is the strain sensor that measures contact at the fingertip.

negligible compared to the magnitude of $\frac{2E}{L}(r + r_t)$. Thus, using a linear fit is reasonable for data analysis. The slope of θ vs. P in $\frac{\text{degree}}{\text{psi}}$ is:

$$\frac{L}{2E(r + r_t)} = 2.7579 \quad (8)$$

Using the linear fit generated from experimental data, the slope is $3.2386 \frac{\text{degree}}{\text{psi}}$ for the 5.08 mm chamber size, and $2.8406 \frac{\text{degree}}{\text{psi}}$ for the 6.35 mm chamber size.

To validate our sensor model, we measured the resistance vs. change in length relationship for multiple sensors (Fig. 9). From equation 7, we know that the ideal behavior of R vs. Δl should be a second order polynomial. However, since the stretched length of the sensor is very small, the second order term Δl^2 has a small effect and thus the first order term Δl dominates. The predicted slope, which is calculated by $\frac{4\rho}{A}$, is $1958 \frac{\text{ohm}}{\text{m}}$. From the linear fit of the data, the slope is $2038 \frac{\text{ohm}}{\text{m}}$. Since the values are similar, we can conclude that a linear model for the sensor is reasonable.

We demonstrated our sensor skin for our specific soft robotic gripper, but this skin approach could be usable for other grippers as well. Several factors can result in differences between our theoretical and experimental results. The major factor is from the uncertainty of the Young's modulus of the actuators. The actual Young's modulus should be lower

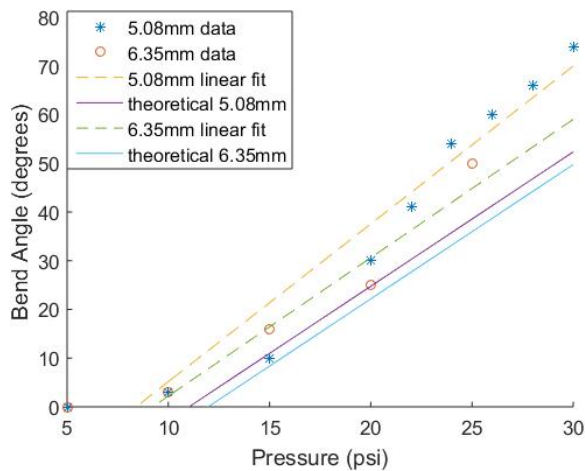


Fig. 8: Plot comparing analytical actuator model, experimental data, and linear fit for the bend angle of the finger modules. Solid lines show the linear model prediction. Dashed lines show the best-fit line to the data. Individual points represent the experimental data. The theoretical model is approximately accurate for pressures at which we actuate our fingers. We assume an input range of 10 psi and above because below that threshold, the pressure does not overcome the elastic restoring forces of the material and thus no inflation occurs.

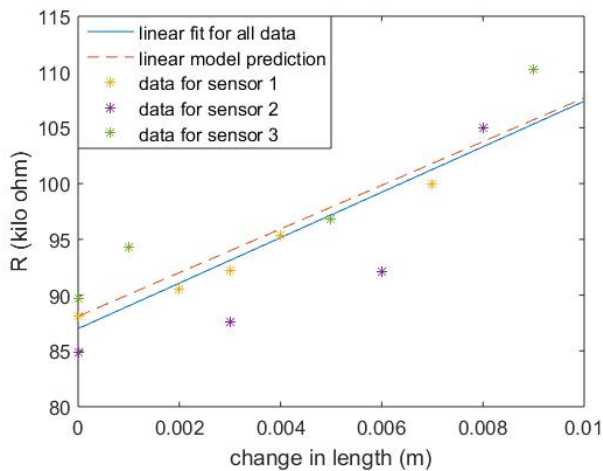


Fig. 9: Plot comparing analytical sensor model, experimental data, and linear fit for the change in resistance of the sensors. Solid lines show the linear model prediction. Dashed lines show the best-fit line for the data. Individual points represent the experimental data.

than the theoretical one because of the other hollow chambers in the actuator. Since the volume fraction of the hollow chamber is approximately 20% to 30% of the total volume of the actuator, the larger slope of the θ vs. P fit is reasonable. In addition, some inhomogeneities may be introduced during the manufacturing process and to the abrupt material strain as the finger begins inflating. Nevertheless, the finger modules

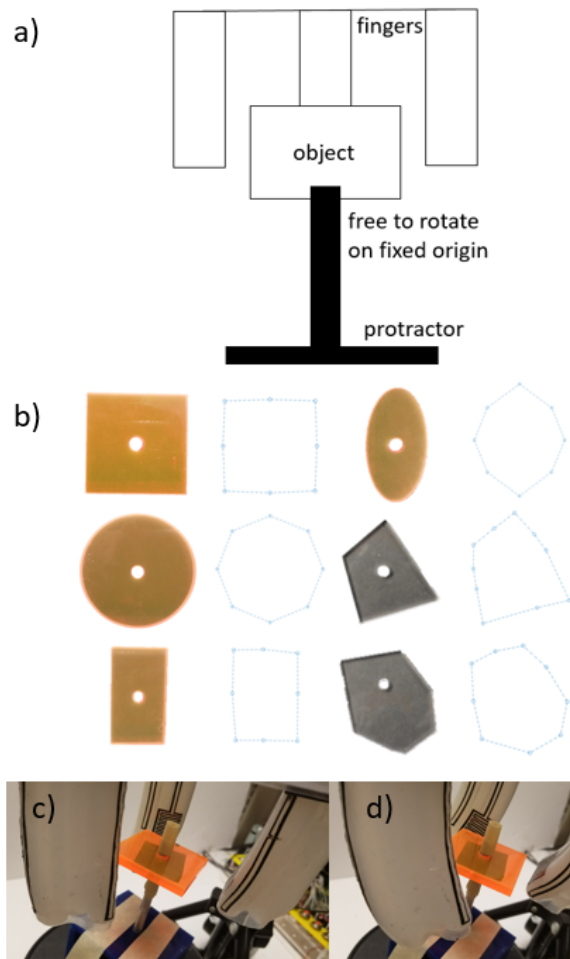


Fig. 10: Setup used for 2D tactile object modeling. a) Side view schematic of how the fingers and object are positioned. We use a protractor as a ground truth for the angle of rotation. b) Our soft gripper is able to model various convex shapes, including square, circle, rectangle, oval, and convex shapes. For each shape, the left is the 2D acrylic piece we used in the modeling experiment and the right is the resulting visualization. We connected the contact points with dotted, straight lines for visualization purposes. c) Gripper in resting position. d) Gripper rotating the object. Protractor not shown.

and sensors provided measurements sufficient for haptic modeling.

B. 2D Tactile Object Modeling

The ability to predict the pose of our actuator enables us to visualize an object's shape by obtaining its 2D outline. To assist with detecting contact on the fingertip, we incorporated a strain sensor pattern on the skin that fits in between chambers C2 and C3 (Fig. 7). This sensor stretches only when the fingertip comes into contact with an object, giving us a signal to identify touch. In addition, the fingertip helped our fingers recognize sharp corners that could fit in between chambers C2 and C3 and would not otherwise be detectable.

We then used the resistance value of the one corresponding bend sensor (B1 in Fig. 7) and the sensor model to determine

the position of the tip of the finger. We also manually recorded the angle of rotation that the object has moved via visual ground truth. Finally, we plotted these (r, θ) points to generate the 2D tactile object model. We summarized this process in the inner while loop of Algorithm 1.

For the 2D demonstration, we constrained the objects in these visualizations to a fixed central axis and selected points of contact relative to a ground truth to visualize both edges and corners (Fig. 10).

C. 3D Tactile Object Modeling

3D visualizations can be generated from multiple 2D outlines by varying the z-axis positioning at which the gripper comes into contact with the objects. We summarized the 3D twisting and measuring procedure in Algorithm 1 and demonstrated this algorithm by attaching our soft gripper to a robot arm (Fig. 1a). The pneumatics and wires are connected to an open source fluidic control board [29]. Fig. 1b shows a resulting visualization where we fixed the light bulb to a stationary axis of rotation.

Algorithm 1 3D Tactile Object Modeling

```

while height of object has not been traversed do
  while object has not been fully rotated do
    Actuate the fingers until each fingertip pressure sensor comes into contact with the object.
    Measure the strain sensor value of a single fingertip.
    Compute and record the displacement distance and corresponding ground truth angle at which we obtain the measurement.
    Rotate the object by twisting with all of the actuators.
  end
  Increment the position of the gripper along the object's z-axis.
end
Model the object outline by plotting each 2D layer with its corresponding z-axis height.

```

Our results from the 2D and 3D haptic object visualization are a first step towards using haptics to map and learn about objects by touch. The capabilities of our current gripper demonstrate that soft fingers with custom sensor skins are a feasible approach. The object models generated by the gripper produce outlines that visually resemble the original shapes. We could potentially use these results for classifying shapes [30]. However, some limitations include being able to recognize the slope of the surface, nonlinear interpolation between contact points, and convex objects. We require additional improvements and quantification to perform tasks like in-hand manipulation or understand the friction and contact properties of unfamiliar objects.

VII. CONCLUSION AND FUTURE WORK

This paper presents soft sensor skins integrated with a soft pneumatic gripper. The gripper uses tactile sensing and twist objects to obtain a three dimensional tactile feedback-based

model of an object. These fingers can deal with unknown, delicate objects without damaging them, as demonstrated by their ability to visualize a light bulb (Fig. 1). Internal sensing addresses the forward kinematics problem in soft robotics of not precisely knowing where the end effectors are. The experiments in this paper demonstrated the grippers's ability to model objects through touch.

Future work could include augmenting our gripper's capability to understand unknown objects. Our model is limited by the size of the fingers of the gripper because the geometry of the fingers fundamentally limits the resolution of the resulting visualization. We have left a full model and characterization of the 3D workspace of each finger and twisting capabilities of the gripper to future work. In addition, more intelligent, in-hand manipulation algorithms that enable our gripper to maintain its grasp on an object throughout manipulation would eliminate the need for a fixed axis of rotation. For these more advanced manipulations, we could integrate additional fingers and multiple sensor readings in varying contact sequences, rather than simply using a single sensor to detect contact for visualization. We could potentially account for some slipping in the grasping, which can result in a different number of data points despite similar cross-section sizes in an object. We also plan to quantify and experiment with a broader set of objects. One current limitation to full autonomy and in-hand manipulation is our need for a ground truth measurement to identify how much the gripper has rotated the object, which could be addressed using an external camera. We could also enhance our tactile object modeling with higher-resolution sensors on the fingertips to improve our knowledge of sloped surfaces and gather rich tactile-based datasets for grasping. Lastly, communication between the microprocessor controlling our soft gripper and the Robot Operating System (ROS) on-board the robot arm is necessary for a fully autonomous system.

ACKNOWLEDGMENT

This work was supported by the Office of Naval Research grant number N000141712062, the UC San Diego Frontiers of Innovation Scholars Program (FISP), and the National Science Foundation Graduate Research Fellowship Grant No. DGE-1144086. The authors would like to thank the members of the Bioinspired Robotics and Design Lab for their insight and help with fabrication, particularly Tom Kalisky, Yueqi Wang, Kyle Gillespie, Kazuya Otani, and Philip deZonia, in addition to Nicholas Farrow from the Correll Lab at the University of Colorado, Boulder for helpful explanations.

REFERENCES

- [1] C. Laschi, B. Mazzolai, and M. Cianchetti, "Soft robotics: Technologies and systems pushing the boundaries of robot abilities," *Science Robotics*, vol. 1, no. 1, p. eaah3690, 2016.
- [2] D. Rus and M. T. Tolley, "Design, fabrication and control of soft robots," *Nature*, vol. 521, no. 7553, pp. 467–475, 2015.
- [3] S. Kim, C. Laschi, and B. Trimmer, "Soft robotics: a bioinspired evolution in robotics," *Trends in biotechnology*, vol. 31, no. 5, pp. 287–294, 2013.
- [4] R. Pfeifer, M. Lungarella, and F. Iida, "The challenges ahead for bio-inspired 'soft' robotics," *Communications of the ACM*, vol. 55, no. 11, pp. 76–87, 2012.

- [5] D. Drotman, S. Jadhav, M. Karimi, M. T. Tolley, *et al.*, “3d printed soft actuators for a legged robot capable of navigating unstructured terrain,” in *Robotics and Automation (ICRA), 2017 IEEE International Conference on*, pp. 5532–5538, IEEE, 2017.
- [6] P. Polygerinos, Z. Wang, K. C. Galloway, R. J. Wood, and C. J. Walsh, “Soft robotic glove for combined assistance and at-home rehabilitation,” *Robotics and Autonomous Systems*, vol. 73, pp. 135–143, 2015.
- [7] H. Zhao, K. O’Brien, S. Li, and R. F. Shepherd, “Optoelectronically innervated soft prosthetic hand via stretchable optical waveguides,” *Science Robotics*, vol. 1, no. 1, p. eaai7529, 2016.
- [8] B. S. Homborg, R. K. Katzschmann, M. R. Dogar, and D. Rus, “Haptic identification of objects using a modular soft robotic gripper,” in *Intelligent Robots and Systems (IROS), 2015 IEEE/RSJ International Conference on*, pp. 1698–1705, IEEE, 2015.
- [9] R. Deimel and O. Brock, “A novel type of compliant and underactuated robotic hand for dexterous grasping,” *The International Journal of Robotics Research*, p. 0278364915592961, 2015.
- [10] K. Suzumori, S. Iikura, and H. Tanaka, “Applying a flexible microactuator to robotic mechanisms,” *Control Systems, IEEE*, vol. 12, no. 1, pp. 21–27, 1992.
- [11] H. Ritter and R. Haschke, “Hands, dexterity, and the brain,” in *Humanoid Robotics and Neuroscience: Science, Engineering and Society*, pp. 49–77, CRC Press, 2014.
- [12] S. Li, H. Zhao, and R. F. Shepherd, “Flexible and stretchable sensors for fluidic elastomer actuated soft robots,” *MRS Bulletin*, vol. 42, no. 2, pp. 138–142, 2017.
- [13] N. Farrow and N. Correll, “A soft pneumatic actuator that can sense grasp and touch,” in *Intelligent Robots and Systems (IROS), 2015 IEEE/RSJ International Conference on*, pp. 2317–2323, IEEE, 2015.
- [14] R. A. Bilodeau, E. L. White, and R. K. Kramer, “Monolithic fabrication of sensors and actuators in a soft robotic gripper,” in *Intelligent Robots and Systems (IROS), 2015 IEEE/RSJ International Conference on*, pp. 2324–2329, IEEE, 2015.
- [15] J. T. Muth, D. M. Vogt, R. L. Truby, Y. Mengüç, D. B. Kolesky, R. J. Wood, and J. A. Lewis, “Embedded 3d printing of strain sensors within highly stretchable elastomers,” *Advanced Materials*, vol. 26, no. 36, pp. 6307–6312, 2014.
- [16] J. Kim, A. Alspach, and K. Yamane, “3d printed soft skin for safe human-robot interaction,” in *Intelligent Robots and Systems (IROS), 2015 IEEE/RSJ International Conference on*, pp. 2419–2425, IEEE, 2015.
- [17] A. M. Okamura, M. L. Turner, and M. R. Cutkosky, “Haptic exploration of objects with rolling and sliding,” in *Robotics and Automation, 1997. Proceedings., 1997 IEEE International Conference on*, vol. 3, pp. 2485–2490, IEEE, 1997.
- [18] H. A. Sonar and J. Paik, “Soft pneumatic actuator skin with piezoelectric sensors for vibrotactile feedback,” *Frontiers in Robotics and AI*, vol. 2, p. 38, 2015.
- [19] N. Gorges, S. E. Navarro, D. Göger, and H. Wörn, “Haptic object recognition using passive joints and haptic key features,” in *Robotics and Automation (ICRA), 2010 IEEE International Conference on*, pp. 2349–2355, IEEE, 2010.
- [20] R. D. P. Wong, R. B. Hellman, and V. J. Santos, “Haptic exploration of fingertip-sized geometric features using a multimodal tactile sensor,” in *SPIE Sensing Technology+ Applications*, pp. 911605–911605, International Society for Optics and Photonics, 2014.
- [21] A. J. Spiers, M. V. Liarokapis, B. Calli, and A. M. Dollar, “Single-grasp object classification and feature extraction with simple robot hands and tactile sensors,” *IEEE transactions on haptics*, vol. 9, no. 2, pp. 207–220, 2016.
- [22] H. Yousef, M. Boukallel, and K. Althoefer, “Tactile sensing for dexterous in-hand manipulation in robotics – a review,” *Sensors and Actuators A: physical*, vol. 167, no. 2, pp. 171–187, 2011.
- [23] R. R. Ma and A. M. Dollar, “On dexterity and dexterous manipulation,” in *Advanced Robotics (ICAR), 2011 15th International Conference on*, pp. 1–7, IEEE, 2011.
- [24] J. Fraś, J. Czarnowski, M. Maciaś, J. Główska, M. Cianchetti, and A. Menciassi, “New stiff-flop module construction idea for improved actuation and sensing,” in *Robotics and Automation (ICRA), 2015 IEEE International Conference on*, pp. 2901–2906, IEEE, 2015.
- [25] S. Sareh, A. Jiang, A. Faragasso, Y. Noh, T. Nanayakkara, P. Dasgupta, L. D. Seneviratne, H. A. Wurdemann, and K. Althoefer, “Bio-inspired tactile sensor sleeve for surgical soft manipulators,” in *Robotics and Automation (ICRA), 2014 IEEE International Conference on*, pp. 1454–1459, IEEE, 2014.
- [26] B. C. Mac Murray, X. An, S. S. Robinson, I. M. van Meerbeek, K. W. O’Brien, H. Zhao, and R. F. Shepherd, “Poroelastic foams for simple fabrication of complex soft robots,” *Advanced Materials*, vol. 27, no. 41, pp. 6334–6340, 2015.
- [27] A. D. Marchese, R. K. Katzschmann, and D. Rus, “A recipe for soft fluidic elastomer robots,” *Soft Robotics*, vol. 2, no. 1, pp. 7–25, 2015.
- [28] C.-X. Liu and J.-W. Choi, “Patterning conductive pdms nanocomposite in an elastomer using microcontact printing,” *Journal of Micromechanics and Microengineering*, vol. 19, no. 8, p. 085019, 2009.
- [29] D. P. Holland, E. J. Park, P. Polygerinos, G. J. Bennett, and C. J. Walsh, “The soft robotics toolkit: Shared resources for research and design,” *Soft Robotics*, vol. 1, no. 3, pp. 224–230, 2014.
- [30] L. d. F. D. Costa and R. M. Cesar Jr, *Shape analysis and classification: theory and practice*. CRC Press, Inc., 2000.